

# Shock Capturing without Riemann Solver – A Modified Space-Time CE/SE Method for Conservation Laws

Zeng-Chan Zhang<sup>1</sup> and Sheng-Tao Yu<sup>2</sup>

Mechanical Engineering Department,  
Wayne State University, Detroit, MI 48202

## ABSTRACT

In this paper, we report an extension of the method of Space-Time Conservation Element and Solution Element, originally developed by Chang [1] for solving conservation laws. In the present method, a single conservation element at each grid point is employed for solving conservation laws in one, two, and three spatial dimensions, instead of two in one-dimensional, three in two-dimensional, and four in three-dimensional problems, as proposed by Chang. As a contrast to Chang's approach, the conservation element here is used to calculate flow variables only, whilst the gradients are calculated by a central-difference type reconstruction method. For equations in one spatial dimension, the present approach is a special case of Chang's  $a$ - $\varepsilon$  scheme. For equations in two and three dimensions, the present method can be easily applied to a regular structured mesh. As such, the present method can serve as an alternative solver for time-accurate solutions in well-established CFD codes. Nevertheless, the present scheme inherits all advantageous features of the original space-time method, including efficient operational count, easiness of implementing non-reflective boundary condition, and high-fidelity resolution of wave motions. In particular, the Godunov type methods using Riemann solvers, i.e., the paradigm of the modern upwind schemes, are not needed to catch shocks. Therefore, the computational logic is considerably simpler. To demonstrate the capability of the new method, numerical results of several benchmark problems are presented, including Sod shock-tube problem, oblique shock reflection, supersonic flows over a forward facing step, and shock/boundary layer interaction.

## 1. INTRODUCTION

Recently, Chang and coworkers [1,2,3] reported a novel numerical framework for solving conservation laws, namely, the method of Space-Time Conservation Element and

Solution Element, or the CE/SE method for short. The method is based on an equal-footing treatment of space and time in calculating flux balance in a space-time domain. The method is not an incremental improvement of a previously existing method and it differs substantially from other well-established CFD methods. The design principles of the CE/SE method have been extensively illustrated in the cited references. Here, only a brief description of the CE/SE method is provided as the background of the present work. In particular, we shall review the conventional integral equation for hyperbolic conservation laws as a contrast to Chang's space-time integral form such that the significance of Chang's space-time formulation can be underlined. To this end, we shall first discuss the Reynolds transport theorem, from which the conventional finite-volume methods were derived. Because space and time are not treated equally, the space-time geometry has been restricted. As discovered by Godunov, the classical Riemann problem was encountered in balancing the space-time flux. Due to an equal footing treatment of space and time, Chang's formula is flexible to allow a better choice of space-time geometry to calculate flux conservation such that the Riemann problem was avoided in balancing the space-time flux.

### 1.1 Reynolds Transport Theorem

The conventional finite-volume methods for simulating the conservation laws were formulated according to flux balance over a *fixed spatial domain*. The conservation laws state that the rate of change of the total amount of a substance contained in a fixed spatial domain  $V$  is equal to the flux of that substance across the boundary of  $V$ , i.e.,  $S(V)$ . Let the density of the substance be  $u$  and its spatial flux be  $f$ , the convection equation can be written as

$$u_t + \bar{\nabla} \cdot f = 0 \quad (1.1)$$

According to the Reynolds transport theorem, the integral form of the above equation can be expressed as:

$$0 = \frac{d}{dt} \int_{V_t} u dV_t = \frac{\partial}{\partial t} \int_{V_t} u dV_t + \int_{S(V_t)} \bar{f} \cdot d\bar{s} \quad (1.2)$$

<sup>1</sup> Visiting Professor, Email: [zz9@nova.eng.wayne.edu](mailto:zz9@nova.eng.wayne.edu)

Permanent address: Department of Engineering Mechanics, Tsinghua University, Beijing 100084, P. R. China

<sup>2</sup> Associate Professor of Mechanical Engineering, AIAA Member, Email: [styu@eng.wayne.edu](mailto:styu@eng.wayne.edu)

where the first term is based on the Lagrangian frame and the right hand side is on the Eulerian frame. The conventional finite-volume methods concentrated on calculating the surface flux in Eq. (1.2), i.e., the last term of Eq. (1.2). The time derivative term of Eq. (1.2) is usually discretized by a finite difference method, e.g., the Runge-Kutta method. Or, integration can be performed for temporal evolution:

$$\int_V u dV \Big|_{t_1}^{t_2} = \int_{t_1}^{t_2} \left( - \int_{S(V)} \vec{f} \cdot d\vec{s} \right) dt \quad (1.3)$$

Due to the *fixed spatial domain*, the shape of the space-time Conservation Elements (CEs) in one spatial dimension for Eq. (1.3) must be rectangular. Refer to Fig. 1.1(a). These elements must stack up exactly on the top of each other in the temporal direction, i.e., no staggering of these elements in time is allowed. For equations in two space dimensions, as depicted in Fig. 1.1(b), a conservation element is a uniform-cross-section cylinder in the space-time domain, and again no staggering in time is allowed.

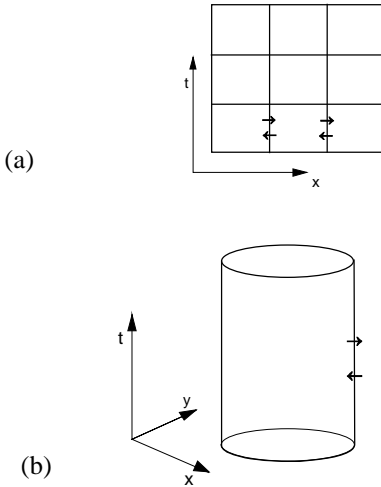


Fig. 1.1 Space-time integration for conventional finite-volume methods

This arrangement results in vertical interfaces extended in the direction of time evolution between adjacent space-time conservation elements. Across these interfaces, flow information travels in both directions. Therefore, an upwind bias method (or a Riemann solver) must be employed to calculate the interfacial fluxes.

## 1.2 Space-Time Integral Form

Consider the following convection equation in the differential form

$$\frac{\partial u_m}{\partial t} + \nabla \cdot \mathbf{f} = 0 \quad (1.4)$$

Where  $\mathbf{f} = (f_x, f_y, f_z)$  is the flux vector. Let  $x_1 = x$ ,  $x_2 = y$ ,  $x_3 = z$ , and  $x_4 = t$  be the four coordinates of a four-dimensional

space-time domain, and the above equation is a divergence free condition, i.e.,

$$\nabla \cdot \mathbf{h} = 0 \quad (1.5)$$

where the current density vector  $\mathbf{h} = (f_x, f_y, f_z, u)$ . According to the divergence theorem, we obtain

$$\oint_{S(V)} \mathbf{h} \cdot d\mathbf{s} = 0 \quad (1.6)$$

Figure 1.2 is a schematic for Eq. (1.6) in one spatial dimension.

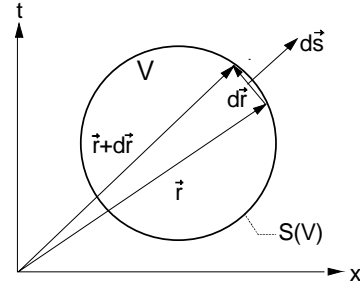


Fig. 1.2 A schematic of Chang's space-time integral form<sup>[1]</sup>.

We remark that space and time are treated in an equal footing manner and therefore there is no restriction on the space-time geometry of the CEs and SEs. Although not shown, similar space-time arrangement is adopted for equations in two and three spatial dimensions.

## 1.3 The *a* Scheme

Based on the above integral equation for space-time flux balance, Chang proposed a new numerical framework for conservation laws, i.e., the CE/SE method. The method is a family of schemes, i.e., the *a* scheme, the *a-ε* scheme, and the *a-α* scheme. The *a* scheme is the backbone of the CE/SE method, and it determines the space-time geometry of the numerical mesh employed. The *a-ε* and the *a-α* schemes are extensions of the *a* scheme for nonlinear equations and for capturing shocks.

In the CE/SE method, the space-time domain of interest is divided into many Solution Elements (SEs). In each SE, flow variables are assumed continuous. According to Chang, a first-order Taylor series is used to represent the discretized flow variables, i.e., a second-order linear distribution. Across the boundaries of neighboring SEs, flow discontinuities are allowed. Flow variables at neighboring mesh points are related only through a local space-time flux balance, which is enforced by integrating over the surfaces of a Conservation Element (CE). Unlike SEs, various CEs could be imposed for local and global space-time flux balance.

In the original  $a$  scheme, the number of the CEs employed in marching the flow solution at one space-time location is equal to the number of unknowns designated by the scheme. In addition to the flow variables, Chang [1] also treated the spatial gradients of flow variables as unknowns. As a result, two CEs are used to solve a one-dimensional flow equations because the flow variable  $u_m$  as well as its spatial derivative  $u_{mx}$  are the unknowns. Note that  $m = 1, 2, 3$  for the three flow variables of the one-dimensional Euler equations. Similarly, three CEs are used for two-dimensional equations because  $u$ ,  $u_{mx}$ , and  $u_{my}$ , are the unknowns. Here  $m = 1, 2, 3, 4$  for the two-dimensional Euler equations. And four CEs are used for three-dimensional flows. Therefore, a triangular mesh must be used for two-dimensional flows and tetrahedrons for three-dimensional flows. Contrary to the reconstruction step of that in a standard upwind scheme, the distribution of flow variables inside a SE are not influenced by its neighboring values at the same time level.

In marching the flow solution, the flow variables at neighboring locations leapfrog each other in time in a zigzagging manner. Refer to Fig. 1.3 for equations in one spatial dimension. This is possible because of a flexible choice of the space-time domain for conservation elements. Through each oblique interface between adjacent SEs, flow information propagates only in one direction towards the future time step. Thus no Riemann problem is encountered and the use of a Riemann solver to catch shocks is avoided.

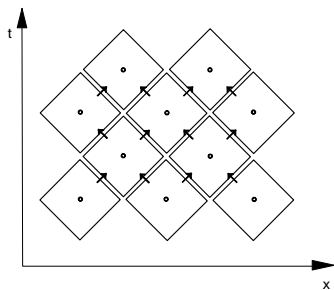


Fig. 1.3 A schematic of the CE/SE method in one spatial dimension.

For the same reason, the treatment of the non-reflective boundary condition in the CE/SE method is very simple [4]. Usually, one simply extrapolates the flow variables to the mesh point in the staggered position at the next time step and a nearly perfect non-reflective boundary condition can be achieved.

In Chang's  $a$ -scheme, the same strategy of space-time flux balance is applied to one-dimensional flows as well as to multi-dimensional flows. No directional splitting or fractional step method is used. Therefore, numerical accuracy does not deteriorate as one moves from one-dimensional flow calculations to multi-dimensional flows. The resultant  $a$  scheme is non-dissipative (or neutrally stable) for linear waves. One can march the solution from a specific space-time point first forward in time and then

backward to recover the initial condition of the flow variables. In other words, the  $a$ -scheme is space-time inversion [ref.6]. In general, lack of space-time inversion of conventional CFD schemes is the cause of the inherent artificial damping.

#### 1.4 The $a$ - $\epsilon$ and $a$ - $\alpha$ Schemes

When dealing with nonlinear equations, e.g., the Euler equations, the above  $a$  scheme must be modified by adding artificial damping for numerical stability. That is the  $a$ - $\epsilon$  scheme. By adding the artificial damping, the calculated values of the gradient, i.e.,  $u_{mx}$ ,  $u_{my}$ , and  $u_{mz}$ , will be altered, while the calculation of  $u_m$  is identical to that of the original  $a$  scheme. When contact discontinuities appear in the flow solution, the calculation of  $u_{mx}$ ,  $u_{my}$ , and  $u_{mz}$  is further modified by a re-weighting function to filter out spurious oscillation caused by the jump, i.e., the  $a$ - $\alpha$  scheme, with  $\alpha$  as the weighting parameter.

Up to date, numerical software based on the CE/SE method for calculating one, two, and three-dimensional flows has been developed. Numerous results were demonstrated, including Sod's shock-tube problem, Lax's problem, Sjogreen's problem, Shu and Osher's problem, merging of two shocks, the shock tube problem with closed end, the implosion and explosion problem, shocks over forward facing step, acoustic waves, shock/acoustic waves interactions -- just to name a few. We have found that numerical resolution of two and three-dimensional shock waves do not deteriorate as compared to that of the one-dimensional shocks. In two-dimensional flows, the resolution of the reflected shocks and shock interactions is as crisp as that of the leading shock. In addition, the method can clearly resolve acoustic waves/shocks interactions while the difference of the magnitude between acoustic waves and shocks could be up to six orders. According to these results, the CE/SE method has proved to be a promising numerical framework for solving fluid dynamics problems.

#### 1.5 The objectives of the Present Work

In the present work, we propose to use different space-time geometry for CEs and SEs. In particular, the number of the unknowns and the number of the CEs employed will not be matched. Instead, only one CE is used at each mesh point to calculate  $u_m$ .

Note that Chang's original  $a$  scheme is non-dissipative and space-time reversible. However, adding the artificial damping is necessary for solving the nonlinear equation as well as for shock capturing. As such, the flow property gradients calculated by the  $a$ - $\alpha$  and  $a$ - $\epsilon$  schemes do not satisfy the space-time flux conservation. That is the property of space-time reversible and non dissipativeness is lost. Thus, the algorithm of calculating the flow property gradients could be modified.

In the present method, the gradients ( $u_{mx}$ ,  $u_{my}$ ,  $u_{mz}$ ) are calculated based on a finite-difference type reconstruction method, which was inspired by Chang's  $a$ - $\varepsilon$  scheme for one-dimensional equations. Because of the finite-difference reconstruction, the present method can be straightforwardly applied to structured mesh for flows in two and three spatial dimensions.

In short, the objective of the present paper is to extend the original space-time method for structured mesh such that this novel space-time approach can be employed as an alternative solver for unsteady flows in well established CFD codes. The rest of the paper is organized as follows. In Section 2, the modified space-time scheme for solving the Euler equations in one, two, and three spatial dimensions will be illustrated. In Section 3, numerical examples obtained by using the present method will be presented. We then offer some concluding remarks.

## 2. NUMERICAL METHODS

### 2.1 The Modified Scheme for the 1D Euler Equations

The one-dimensional Euler equations for a perfect gas are of concern,

$$\partial u_m / \partial t + \partial f_m / \partial x = 0, \quad m=1,2,3 \quad (2.1)$$

Following Chang's equal-footing treatment of space and time, we let  $x_1 = x$  and  $x_2 = t$  be the two coordinates of a two-dimensional Euclidean space  $E_2$ . By using the Gauss divergence theorem in the  $E_2$  space, Eq. (2.1) has the following integral counterpart:

$$\oint_{S(V)} h_m \cdot ds = 0, \quad m=1,2,3 \quad (2.2)$$

Where  $S(V)$  is the boundary of an arbitrary space-time region  $V$  in  $E_2$ , and  $h_m = (f_m, u_m)$  is the space-time current density vector.

The definitions of the conservation element (CE) and the solution element (SE) are of utmost importance in the formulating of the space-time flux conservation. A CE is a small region in  $E_2$ , in which Eq. (2.2) is enforced. A SE is such a small region in  $E_2$  in which the flow variables can be approximated by simple functions. In the original CE/SE method, the number of CEs associated with each grid point must be identical to the number of the unknown variables. In one-dimensional cases, two CEs associated with each grid point are used such that two unknowns  $u_m$  and  $u_{mx}$  at each grid point are solved.

In the present approach, only one CE associated with each grid point is used mainly for solving the unknown variables  $u_m$ . The calculation of  $u_{mx}$  is based on the assumption of continuity of  $u_m^*$  at the common points of neighboring SEs. Thus the discrete equation for solving  $u_{mx}$  can be obtained. This is the main difference between the present scheme and Chang's CE/SE method.

Let  $\Omega$  denotes the set of mesh points  $(j, n)$  in  $E_2$ , i.e., the open circles in Fig. 2.1(a), where  $n = 0, \pm 1/2, \pm 2/2, \dots$ , and  $j = n \pm 1/2, n \pm 3/2, \dots$ . For each mesh point  $(j, n)$ , the CE is defined as the square  $BCEF$ , and the SE is the interior of the rhombus  $BDFG$ . Refer to Fig. 2.1(b).

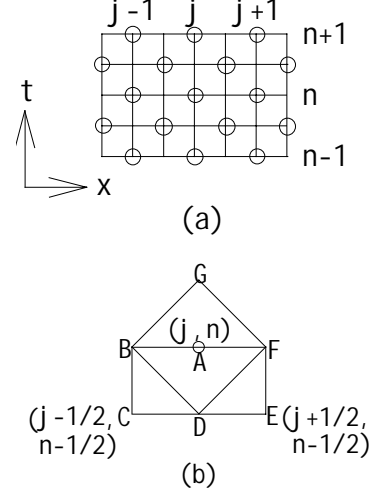


Fig. 2.1 The mesh and the definitions of SEs and CEs

By the definition of SE, for any  $(x, t) \in SE(j, n)$ ,  $u_m(x, t)$  and  $f_m(x, t)$  can be respectively approximated by their discrete counterparts, i.e.,  $u_m^*(x, t; j, n)$  and  $f_m^*(x, t; j, n)$ . Using the first-order Taylor expansion, we have

$$u_m^*(x, t; j, n) = (u_m)_j^n + (u_{mx})_j^n (x - x_j) + (u_{mt})_j^n (t - t^n), \quad (2.3)$$

$$f_m^*(x, t; j, n) = (f_m)_j^n + (f_{mx})_j^n (x - x_j) + (f_{mt})_j^n (t - t^n). \quad (2.4)$$

Accordingly,

$$h_m^*(x, t; j, n) = (f_m^*(x, t; j, n), u_m^*(x, t; j, n)). \quad (2.5)$$

Equation (2.2) can then be approximated by the discrete form:

$$\oint_{S(CE(j,n))} h_m^* \cdot ds = 0, \quad \forall (j, n) \in \Omega \quad (2.6)$$

Substitute  $u_m = u_m^*(x, y, t; i, j, n)$  and  $f_m = f_m^*(x, y, t; i, j, n)$  into Eq. (2.1) and we get

$$(u_{mt})_{i,j}^n = -(f_{mx})_{i,j}^n \quad (2.7)$$

As a result, the only independent discrete variables needed to be solved are  $u_m$  and  $u_{mx}$ . Substituting Eqs. (2.3-5) into Eq. (2.6), one concludes that:

$$(u_m)_j^n = [(u_m)_{j-1/2}^{n-1/2} + (u_m)_{j+1/2}^{n-1/2} + (s_m)_{j-1/2}^{n-1/2} - (s_m)_{j+1/2}^{n-1/2}] / 2, \quad (2.8)$$

where

$$(s_m)_j^n = (\Delta x / 4)(u_{mx})_j^n + (\Delta t / \Delta x)(f_m)_j^n + (\Delta t^2 / 4\Delta x)(f_{mt})_j^n.$$

Equation (2.8) is the algorithm for solving  $u_m$ . Note that Eq. (2.8) is identical to Chang's formulation. Interested readers are referred to [1] for details.

To solve for  $u_{mx}$ , the numerical continuity of  $u_m^*$  at the grid points B and F of the two neighboring SEs is assumed. Refer to Fig. 2.1(b). As such, the variable gradient at the  $(n, j)$  point can be calculated by the central difference method, i.e.,

$$(u_{mx})_j^n = [(u_{mx}^+)_j^n + (u_{mx}^-)_j^n] / 2 \quad (2.9)$$

where

$$(u_{mx}^\pm)_j^n = \pm [(u_m^+)_j^{n+1/2} - (u_m^-)_j^n] / (\Delta x / 2),$$

$$(u_m^+)_j^{n+1/2} = (u_m^-)_j^{n-1/2} + (\Delta t / 2)(u_{mt})_j^{n-1/2}.$$

Equations (2.8) and (2.9) are the modified space-time conservation scheme for the one-dimensional Euler equations. We remark that this scheme is a special case of Chang's  $\alpha$ - $\varepsilon$  scheme for  $\varepsilon=0.5$ . Therefore, according to Chang's analysis, the present scheme is second-order, and the stability condition is  $CFL \leq 1$ . For flows with discontinuities, Eq. (2.9) is further modified by the following re-weighting procedure

$$(u_{mx})_j^n = W((u_{mx}^-)_j^n, (u_{mx}^+)_j^n, \alpha), \quad (2.9)'$$

The re-weighting function  $W$  is defined by

$$W(x_-, x_+, \alpha) = \frac{[|x_+|^\alpha x_- + |x_-|^\alpha x_+]}{[|x_+|^\alpha + |x_-|^\alpha]},$$

where  $\alpha$  is an adjustable constant, and usually  $\alpha = 1$  or  $2$ . The above re-weighting function is a simple limiter for  $u_{mx}$  to suppress spurious oscillations near shocks.

## 2.2 The Modified Scheme for the 2D Euler Equations

The two-dimensional Euler equations of a perfect gas are of concern,

$$\frac{\partial u_m}{\partial t} + \frac{\partial f_m}{\partial x} + \frac{\partial g_m}{\partial y} = 0, \quad m=1,2,3,4 \quad (2.10)$$

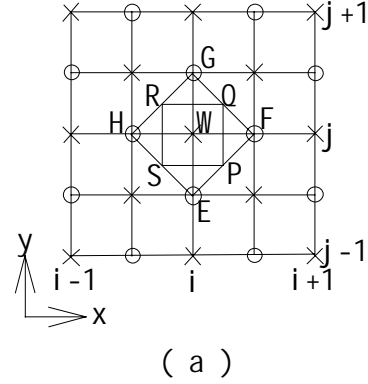
Let  $x_1 = x$ ,  $x_2 = y$ , and  $x_3 = t$  be the coordinates of a three-dimensional Euclidean space  $E_3$ . Using Gauss' divergence theorem, we obtain the following integral equations

$$\oint_{S(V)} h_m \cdot ds = 0, \quad m=1,2,3,4 \quad (2.11)$$

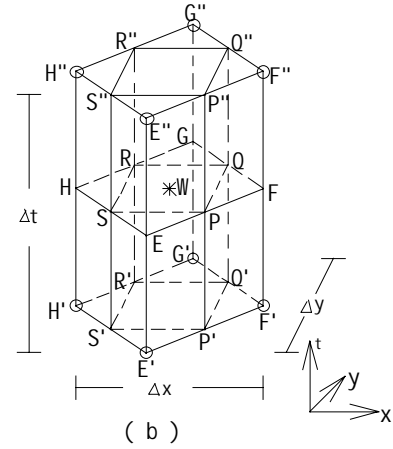
Where  $S(V)$  is the boundary of a space-time region  $V$ , and  $h_m = (f_m, g_m, u_m)$  is the space-time current density vector. In the original CE/SE method, three CEs are used at each mesh point to provide three conditions for three unknowns,  $u$ ,  $u_{mx}$ , and  $u_{my}$ . As a result, triangular mesh must be employed.

In the present approach, the mesh arrangement in the  $x$ - $y$  plane is depicted in Fig. 2.2(a). There are two groups of grid points, marked by open circles and crosses, representing mesh points at two consecutive semi-time. Let  $\Omega$  denote the set of mesh points  $(i, j, n)$  in  $E_3$ , with  $n, j=0, \pm 1/2, \pm 2/2, \dots$ , and  $i=n+j\pm 0, n+j\pm 1, \dots$ . There is one CE and one SE associated with each mesh point  $(i, j, n)$ . Here

the CE is the quadrilateral cylinder  $EFGHE'F'G'H'$ , and the SE is the union of the quadrilateral cylinder  $P''Q''R''S''P'Q'R'S'$  in conjunction with the horizontal plane  $EFGH$ . Refer to Fig. 2.2(b).



( a )



( b )

Fig.2.2 The representative grid points in  $x$ - $y$  plane and the definitions of SE and CE

For any  $(x, y, t)$  inside the  $SE(i, j, n)$ , the first order Taylor series expansion is used to approximate the  $u_m(x, y, t)$ ,  $f_m(x, y, t)$ , and  $g_m(x, y, t)$ , i.e.,

$$u_m^*(x, y, t; i, j, n) = (u_m)_{i,j}^n + (u_{mx})_{i,j}^n(x - x_i) + (u_{my})_{i,j}^n(y - y_j) + (u_{mt})_{i,j}^n(t - t^n) \quad (2.12)$$

$$f_m^*(x, y, t; i, j, n) = (f_m)_{i,j}^n + (f_{mx})_{i,j}^n(x - x_i) + (f_{my})_{i,j}^n(y - y_j) + (f_{mt})_{i,j}^n(t - t^n) \quad (2.13)$$

$$g_m^*(x, y, t; i, j, n) = (g_m)_{i,j}^n + (g_{mx})_{i,j}^n(x - x_i) + (g_{my})_{i,j}^n(y - y_j) + (g_{mt})_{i,j}^n(t - t^n) \quad (2.14)$$

Because  $h_m = (f_m, g_m, u_m)$ , we have

$$h_m^*(x, y, t; i, j, n) = (f_m^*(x, y, t; i, j, n), g_m^*(x, y, t; i, j, n), u_m^*(x, y, t; i, j, n)) \quad (2.15)$$

The discrete form of Eq. (2.11) can then be represented as

$$\oint_{S(CE(i,j,n))} h_m^* \cdot ds = 0, \quad \forall (i, j, n) \in \Omega \quad (2.16)$$

Substitute  $u_m = u_m^*(x, y, t; i, j, n)$ ,  $f_m = f_m^*(x, y, t; i, j, n)$ , and  $g_m = g_m^*(x, y, t; i, j, n)$  into Eq. (2.10), and we have

$$(u_m)_{i,j}^n = -(f_{mx})_{i,j}^n - (g_{my})_{i,j}^n \quad (2.17)$$

Thus, the unknowns at each grid point need to be solved are  $u_m$ ,  $u_{mx}$  and  $u_{my}$ . Substituting Eqs. (2.12-15) into Eq. (2.16), we obtain

$$(u_m)_{i,j}^n = \left\{ Q_m^{(1)}(-\Delta x / 2) \right\}_{i-1/2,j}^{n-1/2} + \left\{ Q_m^{(1)}(\Delta x / 2) \right\}_{i+1/2,j}^{n-1/2} \\ + \left\{ Q_m^{(2)}(\Delta y / 2) \right\}_{i,j+1/2}^{n-1/2} + \left\{ Q_m^{(2)}(-\Delta y / 2) \right\}_{i,j-1/2}^{n-1/2} \quad (2.18)$$

where

$$Q_m^{(1)}(\Delta x) = \{(2u_m - \Delta x \cdot u_{mx}) - \Delta t / 2 \cdot [g_{my} + (4f_m - \Delta x \cdot f_{mx} + \Delta t \cdot f_{mt}) / \Delta x]\} / 8$$

$$Q_m^{(2)}(\Delta y) = \{(2u_m - \Delta y \cdot u_{my}) - \Delta t / 2 \cdot [f_{mx} + (4g_m - \Delta y \cdot g_{my} + \Delta t \cdot g_{mt}) / \Delta y]\} / 8$$

To proceed, we assume the value of  $u_m^*$  from different SEs at the common grid points E, F, G and H are the same. Refer to Fig. 2.2(b). As a result, one has:

$$(u_{mx})_{i,j}^n = [(u_{mx}^+)_{i,j}^n + (u_{mx}^-)_{i,j}^n] / 2 \quad (2.19a)$$

$$(u_{my})_{i,j}^n = [(u_{my}^+)_{i,j}^n + (u_{my}^-)_{i,j}^n] / 2 \quad (2.19b)$$

where

$$(u_{mx}^\pm)_{i,j}^n = \pm [(u_m^{\cdot})_{i\pm 1/2,j}^n - (u_m)_{i,j}^n] / (\Delta x / 2)$$

$$(u_{my}^\pm)_{i,j}^n = \pm [(u_m^{\cdot})_{i,j\pm 1/2}^n - (u_m)_{i,j}^n] / (\Delta y / 2)$$

$$(u_m^{\cdot})_{i\pm 1/2,j}^n = \left\{ u_m + \Delta t \cdot u_{mt} / 2 \right\}_{i\pm 1/2,j}^{n-1/2}$$

$$(u_m^{\cdot})_{i,j\pm 1/2}^n = \left\{ u_m + \Delta t \cdot u_{mt} / 2 \right\}_{i,j\pm 1/2}^{n-1/2}$$

To catch shocks, the gradients of the flow variables are further modified by the re-weighting procedure

$$(u_{mx})_{i,j}^n = W((u_{mx}^-)_{i,j}^n, (u_{mx}^+)_{i,j}^n, \alpha)$$

$$(u_{my})_{i,j}^n = W((u_{my}^-)_{i,j}^n, (u_{my}^+)_{i,j}^n, \alpha)$$

This concludes the discussion of the modified space-time conservation scheme for the 2-D Euler equations. We remark that other definitions of the CEs and SEs are possible. The one in the above discussion is a natural extension from the scheme for one spatial dimension.

### 2.3 The Modified Scheme for the 3D Euler Equations

The three-dimensional unsteady Euler equations of a perfect gas are of concern,

$$\partial u_m / \partial t + \partial f_m / \partial x + \partial g_m / \partial y + \partial h_m / \partial z = 0, \quad (2.20)$$

$m = 1, 2, 3, 4, 5$ . Let  $x_1 = x$ ,  $x_2 = y$ ,  $x_3 = z$ , and  $x_4 = t$  be the coordinates of a four-dimensional Euclidean space  $E_4$ . The corresponding integral equations of Eq. (2.20) are:

$$\oint_{S(V)} H_m \cdot ds = 0, \quad m=1,2,3,4,5 \quad (2.21)$$

Where  $S(V)$  is the boundary of an arbitrary space-time region  $V$  in  $E_4$ , and  $H_m = (f_{mv}, g_{mv}, h_{mv}, u_m)$ .

Using the similar method of the above sections, we can get the following space-time conservation scheme for the three-dimensional Euler equations:

$$(u_m)_{i,j,k}^n = \{ [Q_m^{(1)}(\Delta x / 2)]_{i+1/2,j,k}^{n-1/2} + [Q_m^{(1)}(-\Delta x / 2)]_{i-1/2,j,k}^{n-1/2} + [Q_m^{(2)}(\Delta y / 2)]_{i,j+1/2,k}^{n-1/2} \\ + [Q_m^{(2)}(-\Delta y / 2)]_{i,j-1/2,k}^{n-1/2} + [Q_m^{(3)}(\Delta z / 2)]_{i,j,k+1/2}^{n-1/2} + [Q_m^{(3)}(-\Delta z / 2)]_{i,j,k-1/2}^{n-1/2} \} / 6 \quad (2.22)$$

and

$$(u_{ml})_{i,j,k}^n = [(u_{ml}^+)_{i,j,k}^n + (u_{ml}^-)_{i,j,k}^n] / 2, \quad l=x, y, z \quad (2.23)$$

or

$$(u_{ml})_{i,j,k}^n = W((u_{ml}^-)_{i,j,k}^n, (u_{ml}^+)_{i,j,k}^n, \alpha), \quad l=x, y, z \quad (2.23)'$$

where

$$Q_m^{(1)}(\beta) = (u_m - \beta / 2 \cdot u_{mx}) - \Delta t / 4 \cdot (g_{my} + h_{mz}) \\ - 3\Delta t / (2\beta) \cdot (f_m - \beta / 3 \cdot f_{mx} + \Delta t / 4 \cdot f_{mt})$$

$$Q_m^{(2)}(\beta) = (u_m - \beta / 2 \cdot u_{my}) - \Delta t / 4 \cdot (h_{mz} + f_{mx}) \\ - 3\Delta t / (2\beta) \cdot (g_m - \beta / 3 \cdot g_{my} + \Delta t / 4 \cdot g_{mt})$$

$$Q_m^{(3)}(\beta) = (u_m - \beta / 2 \cdot u_{mz}) - \Delta t / 4 \cdot (f_{mx} + g_{my}) \\ - 3\Delta t / (2\beta) \cdot (h_m - \beta / 3 \cdot h_{mz} + \Delta t / 4 \cdot h_{mt})$$

$$(u_{mx}^\pm)_{i,j,k}^n = \pm [(u_m^{\cdot})_{i\pm 1/2,j,k}^n - (u_m)_{i,j,k}^n] / (\Delta x / 2);$$

$$(u_{my}^\pm)_{i,j,k}^n = \pm [(u_m^{\cdot})_{i,j\pm 1/2,k}^n - (u_m)_{i,j,k}^n] / (\Delta y / 2)$$

$$(u_{mz}^\pm)_{i,j,k}^n = \pm [(u_m^{\cdot})_{i,j,k\pm 1/2}^n - (u_m)_{i,j,k}^n] / (\Delta z / 2),$$

$$(u_m^{\cdot})_{i\pm 1/2,j,k}^n = \left\{ u_m + \Delta t \cdot u_{mt} / 2 \right\}_{i\pm 1/2,j,k}^{n-1/2}$$

$$(u_m^{\cdot})_{i,j\pm 1/2,k}^n = \left\{ u_m + \Delta t \cdot u_{mt} / 2 \right\}_{i,j\pm 1/2,k}^{n-1/2};$$

$$(u_m^{\cdot})_{i,j,k\pm 1/2}^n = \left\{ u_m + \Delta t \cdot u_{mt} / 2 \right\}_{i,j,k\pm 1/2}^{n-1/2}$$

This concludes the discussion of the three-dimensional space-time conservation scheme for the Euler equations.

## 3. NUMERICAL RESULTS

To demonstrate the capability of this new scheme, several benchmark flow problems are reported here. In the following examples, boundary conditions are specified at inlet surface.

At the outlet surface, the space-time non-reflective condition [14] are used. Along solid boundary, the reflective condition is used.

**Example 1 Sod's Shock Tube Problem [7]**

The computational domain and the flow condition are the same as that in Ref. [1]. Here,  $\Delta t=0.2 \times 10^{-2}$ ,  $\Delta x=0.6 \times 10^{-2}$ , and  $CFL \approx 0.72$ . Figure 3.1 is the velocity distribution at  $t=0.2$ . The solid line is the exact solution and the dots are the numerical solution. It is clear that the shock jump condition is well resolved by only one data point in the shock.

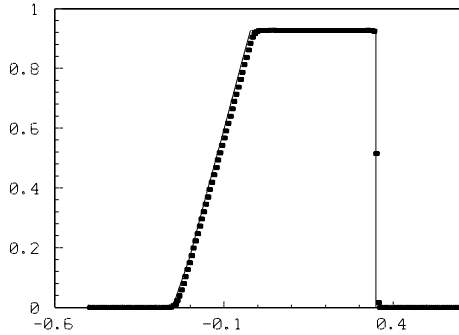


Fig.3.1 The Euler solution of a 1D unsteady shock tube problem

**Example 2 Steady-State Shock Reflection [8]**

The computational domain and the flow condition are the same as that in Ref. [8]. The lower boundary is a solid wall. The size of computational mesh is  $121 \times 81$ . The grid points of the mesh are uniformly distributed. This problem has an exact analytical solution. The computed pressure contours is shown in Fig. 3.2.

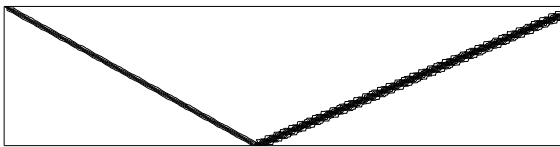


Fig.3.2 Pressure contours of steady-state shock reflection problem

Across the shock, there are about one to two mesh nodes inside the shock. The angle of the reflected shock is very accurate. Although not shown, the numerical result of the pressure jumps agrees well with the exact solution.

**Example 3 Shock over a Forward facing Step**

The geometry of the forward facing step and the flow condition are the same as that in Ref. [9]. The mesh density is  $181 \times 121$ , and the grid points are uniformly distributed. The time increment of the present calculation is  $\Delta t=0.0025$ .

In Fig. 3.3, the computed density contours are plotted for  $t=4$ . In the present numerical solution, the Mach stem, triple point, slip surface, expansion fan at the corner, and the interaction between the reflected shock with rarefaction waves are all accurately simulated. We remark that there is no special treatment at the corner of the step, which is usually required for conventional CFD methods to ensure numerical stability.

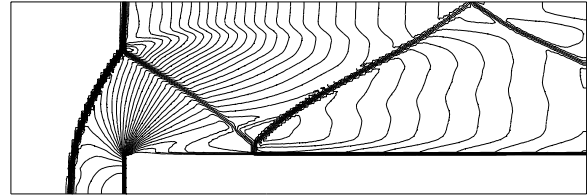


Fig.3.3 Density contours of a two-dimensional supersonic flow passing a forward facing step ( $t=4$ )

**Example 4 Shock/Boundary Layer Interaction [13]**

In this paper, the presentation of this new numerical scheme has been focused on the solution of the Euler equations. Nevertheless, the present scheme can be straightforwardly extended to that for solving the Navier-Stokes equations. The details of this extension will be reported in another paper. Here, a numerical example is provided to demonstrate the applicability of the present scheme to the Navier-Stokes equations.

The flow condition are the same as that reported in Ref. [13]. That is,  $M_\infty = 2.0$ ,  $Re = 2.96 \times 10^5$ ,  $T_\infty = 117$  K, and the incident shock angle is  $\beta = 32.6^\circ$ . A  $180 \times 180$  non-uniform mesh is employed. The mesh is cluster to the wall to resolve the high gradient of velocity inside the boundary layer. The smallest  $\Delta y$  is about  $10^{-3}$ . The characteristic length for nondimensionalization is the distance between the leading edge of the flat plate and the shock incident point. Figure 3.5 is the pressure contours. Due to the Strong incident shock, a separation occurs near the impingement point of the incident shock. The overall flow pattern shown in Fig. 3.4 agrees well with the experiment results [13].

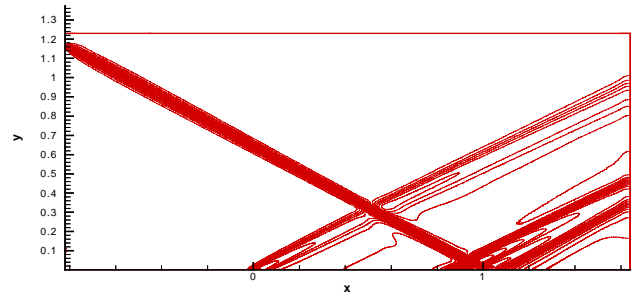


Fig.3.4 The pressure contours of the oblique shock / flat plate boundary layer interaction.

We remark that although not shown, the detailed comparison of pressure and skin friction coefficient  $C_f$  profiles along the solid wall boundary between the numerical results and the experimental data agree very well. These results will be reported in another paper.

#### 4. CONCLUDING REMARKS

In this paper, a modified space-time conservation scheme for solving one, two and three-dimensional Euler equations is reported. In the present approach, only one CE at each mesh point is used to calculate the flow variables. The gradients of the flow variables are calculated by using a central-difference type reconstruction procedure. The present scheme maintains all the favorable features of the original CE/SE method. The calculation of the present scheme is simple, accurate, and can be easily applied to a regular structured mesh. To demonstrate the capability of the present approach, several benchmark problems were calculated. The performance of the present method is satisfactory.

#### ACKNOWLEDGEMENT

This work is performed under the support of NASA Lewis Research Center NCC3-580, monitored by Dr. Philip Jorgenson. This work is also a part of an ongoing program at Wayne State University in applying the Space-Time CE/SE Method to practical engineering problems.

#### REFERENCES

1. Chang, S.C., "The Method of Space-Time Conservation Element and Solution Element – A New Approach for Solving the Navier Stokes and Euler Equations," *J. Comp. Phys.*, Vol. 119, 1995, pp. 295-324
2. Wang, X.Y., Chow, C.Y. and Chang, S.C., "An Euler Solver based on the Method of Space-Time Conservation Element and Solution Element," Proceeding of the 15th Int. Conf. Num. Methods Fluid Dynamics, Monterey, CA, 1996
3. Yu, S.T. and Chang, S.C., "Treatments of Stiff Source Terms in Conservation Laws by the Method of Space-Time Conservation Element and Solution Element," AIAA Paper 97-0435, 1997.
4. Yu, S.T. and Chang, S.C., "Applications of the Space-Time Conservation Element and Solution Element Method to Unsteady Chemically Reactive Flows," AIAA Paper 97-2007, 1997.
5. Loh, C.Y. and Chang, S.C., Scott, J.R. and Yu, S.T., "Application of the Space-Time Conservation Element and Solution Element to Aeroacoustics Problems," AIAA Paper 96-0276, 1996.
6. Chang, S.C., "New Developments in the Method of the Space-Time Conservation Element and Solution Element – Applications to the Euler and Navier-Stokes Equations," NASA TM 106226, 1993.
7. Sod, G. A., "A Survey of Several Finite Difference Method for Systems of Nonlinear Hyperbolic Conservation Laws," *J. Comput. Phys.*, Vol. 27, No.1, 1978, pp. 1-31
8. Chang, S.C., Wang, X.Y. and Chow, C.Y., "The Method of Space-Time Conservation Element and Solution Element – Applications to One and Two-Dimensional Time-Marching Flow Problems," AIAA Paper 95-1754, 1995.
9. Wang, X.Y., "Computational Fluid Dynamics based on the Method of Space-Time Conservation Element and Solution Element," Ph.D. Dissertation, Univ. of Colorado at Boulder, 1995.
10. Nessyahu, H. and Tadmor, E., "Non-Oscillatory Central Differencing of Hyperbolic Conservation laws," *J. Comput. Phys.*, Vol. 87, 1990, pp. 408-463.
11. Sander, R. and Weiser, A., "High Resolution Staggered Mesh Approach for Nonlinear Hyperbolic Systems of Conservation Laws," *J. Comput. Phys.*, Vol. 101, 1992, pp. 314-329.
12. Jiang, G.S., and Tadmor, E., "Non-Oscillatory Central Schemes for Multidimensional Hyperbolic Conservation Laws," UCLA CAM Report 96-36, October 1996.
13. Hakkinen, R.J., Greber, I., Trilling, L. and Abarbanel, S.S., "The Interaction of an Oblique Shock Wave with a Laminar Boundary Layer," NASA Memo 2-18-59W, 1959.
14. Chang, S.C., Himansu, A., Loh, C.Y., Wang, X.Y., Yu S.T., Jorgenson, P., "Robust and Simple Nonreflecting Boundary Conditions for the Space-Time Conservation Element and Solution Element Method," AIAA Paper 97-2077, the 13<sup>th</sup> AIAA CFD Conference, June 1997, Snow Mass, CO.